Atmos. Chem. Phys. Discuss., 14, 18461–18497, 2014
www.atmos-chem-phys-discuss.net/14/18461/2014/
doi:10.5194/acpd-14-18461-2014

Atmospheric Chemistry and Physics Discussions

Fast transport from Southeast Asia boundary layer sources to Northern Europe: rapid uplift in typhoons and eastward eddy shedding of the Asian monsoon anticyclone

B. Vogel[1], G. Günther[1], R. Müller[1], J.-U. Grooß[1], P. Hoor[2], M. Krämer[1], S. Müller[2], A. Zahn[3], and M. Riese[1]

[1]Forschungszentrum Jülich, Institute of Energy and Climate Research – Stratosphere (IEK-7), Jülich, Germany
[2]Institute for Atmospheric Physics, University of Mainz, Mainz, Germany
[3]Institute for Meteorology and Climate Research, Karlsruhe Institute of Technology, Karlsruhe, Germany

Received: 11 June 2014 – Accepted: 29 June 2014 – Published: 11 July 2014

Correspondence to: B. Vogel (b.vogel@fz-juelich.de)

Published by Copernicus Publications on behalf of the European Geosciences Union.

Abstract

During the TACTS aircraft campaign enhanced tropospheric trace gases such as CO, CH_4, and H_2O and reduced stratospheric O_3 were measured in situ in the lowermost stratosphere over Northern Europe on 26 September 2012. The measurements indicate that these air masses differ from the stratospheric background. The calculation of 40 day backward trajectories with the trajectory module of the CLaMS model shows that these air masses are affected by the Asian monsoon anticyclone. Some air masses originate from the boundary layer in Southeast Asia/West Pacific and are rapidly lifted (1–2 days) within a typhoon. Afterwards they are injected directly into the anticyclonic circulation of the Asian monsoon. The subsequent long-range transport (8–14 days) of enhanced water vapour and pollutants to the lowermost stratosphere in Northern Europe is driven by eastward transport of tropospheric air from the Asian monsoon anticyclone caused by an eddy shedding event. We find that the combination of rapid uplift by a typhoon and eastward eddy shedding from the Asian monsoon anticyclone is an additional fast transport pathway that, in this study, carries boundary emissions from Southeast Asia/West Pacific within approximately 5 weeks to the lowermost stratosphere in Northern Europe.

1 Introduction

One of the most pronounced circulation patterns in the the upper troposphere and lower stratosphere (UTLS) during boreal summer is the Asian summer monsoon circulation. It consists of a large-scale anticyclone in the UTLS extending from Asia to the Middle East from early June until end of September. The Asian monsoon anticyclone extends into the lowermost stratosphere (e.g., Randel and Park, 2006), where the tropopause above the monsoon is higher than in the extra-tropics by about 50 K (e.g., Dunkerton, 1995; Highwood and Hoskins, 1998). The anticyclone is flanked by an equatorial east-

ACPD
14, 18461–18497, 2014

erly jet to the south and by the subtropical westerly jet to the north and characterised by low values of Potential Vorticity (PV) (e.g., Randel and Park, 2006).

In general, the Asian monsoon circulation provides an effective pathway for water vapour (Ploeger et al., 2013) and pollutants to the lower stratosphere of the Northern Hemisphere. Water vapour H_2O is the most important greenhouse gas and moistening of the stratosphere is an important driver of climate change (e.g., Forster and Shine, 1999, 2002; Shindell, 2001; Smith et al., 2001; Vogel et al., 2012). In particular, small changes of H_2O in the UTLS have an impact on surface climate (e.g., Solomon et al., 2010; Riese et al., 2012). In spite of its radiative importance changes and trends in UTLS water vapour are only poorly quantified (e.g., Hurst et al., 2011; Kunz et al., 2013). Further, increasing amounts of the greenhouse gas methane (CH_4), in addition, enhance stratospheric water vapour concentrations by methane oxidation (e.g., Röckmann et al., 2004; Riese et al., 2006; Rohs et al., 2006). Methane emissions by rice paddies in India and Southeast Asia (e.g., Khalil et al., 1998; Huang et al., 2004) may provide an important contribution to stratospheric CH_4 in this context. Enhanced water vapour concentrations in the UTLS affect not only the radiative balance, but have also the potential to affect stratospheric chemistry (e.g., Kirk-Davidoff et al., 1999; Dvortsov and Solomon, 2001; Vogel et al., 2011a). An increasing population and growing industries in Asia have the potential to enhance future entry concentrations of water vapour and pollutants into the stratosphere caused by the Asian monsoon anticyclone. Therefore it is important to identify transport pathways to the global stratosphere to allow potential environmental risks to be assessed.

The Asian summer monsoon is associated with strong upward transport of tropospheric source gases by deep convection which is confined by the strong anticyclonic circulation (e.g., Li et al., 2005; Randel and Park, 2006; Park et al., 2007, 2008, 2009). Hence, in satellite measurements relatively large concentrations of tropospheric trace gases such as water vapour (H_2O) (Rosenlof et al., 1997; Jackson et al., 1998), carbon monoxide (CO) (Li et al., 2005; Park et al., 2008), and methane (CH_4) (Park et al., 2004; Xiong et al., 2009) are found in the Asian monsoon anticyclone isolated by a transport

ACPD
14, 18461–18497, 2014

barrier from the surrounding air. Vice versa stratospheric trace gases such as O_3 (Randel and Park, 2006; Liu et al., 2009; Konopka et al., 2010) show low concentrations in the anticyclone. However, the impact of different boundary layer sources on the chemical composition of the air in the Asian monsoon anticyclone (e.g., Li et al., 2005; Park et al., 2009; Chen et al., 2012; Bergman et al., 2013) and the mechanisms for transport into the lowermost stratosphere (Dethof et al., 1999; Park et al., 2009; Randel et al., 2010; Bourassa et al., 2012) are subject of current debate.

Trajectory calculations suggest air mass contributions in the Asian monsoon anticyclone from boundary sources originating in India/Southeast Asia (including the Bay of Bengal) and the Tibetan Plateau (Chen et al., 2012; Bergman et al., 2013). Chen et al. (2012) found the main contribution to air at tropopause height from the tropical Western Pacific region and the South China Seas, while Bergman et al. (2013) found that contributions from the Tibetan Plateau are most important at 100 hPa. In the Asian monsoon, findings by Chen et al. (2012) indicate that timescales of transport from the boundary layer to the tropopause region by deep convection overshooting are about 1–2 days, while several weeks by large scale ascent. Further, there is evidence that emissions on the eastern side of the anticyclone (northeast India and southwest China) are lifted upward and trapped in the Asian monsoon anticyclone (Li et al., 2005).

There is evidence that the mean upward transport at the eastern/southeastern side of the Asian monsoon anticyclone is a gateway of tropospheric air to the stratosphere by direct convective injection (Rosenlof et al., 1997; Park et al., 2007, 2008; Chen et al., 2012). However, the impact of this effect on the composition of the stratosphere has not been isolated from the influence of the transport in the deep tropics, entrained into the upward Brewer–Dobson circulation (Gettelman et al., 2004; Bannister et al., 2004), which is the primary transport pathway of air from the troposphere to the stratosphere (Holton et al., 1995).

One of the possible pathways for long-range transport of air masses from the Asian monsoon anticyclone to the extratropical lowermost stratosphere are smaller anticyclones breaking off a few times each summer from the main anticyclone characterised

ACPD
14, 18461–18497, 2014

by low PV values (Hsu and Plumb, 2001; Popovic and Plumb, 2001; Garny and Randel, 2013). This process is referred to as "eddy shedding". Westward transport of monsoon air masses by eddy shedding from the Asian monsoon anticyclone seems to be a common phenomenon, in contrast to eastward migrating anticyclones that occur less frequently (Popovic and Plumb, 2001; Garny and Randel, 2013). Garny and Randel (2013) found that westward propagation often appear after periods of strong convective forcing. Hsu and Plumb (2001) inferred from shallow-water calculations that in case the anticyclone is sufficiently large asymmetric, the elongated anticyclone becomes unstable and westward eddy shedding occurred. In contrast, eastward eddy shedding is ascribed to the interaction of the monsoon anticyclone with an eastward moving mid-latitude synoptic-scale tropospheric cyclone (Dethof et al., 1999).

Eddy shedding events have the potential to carry air with enhanced tropospheric trace gases such as water vapour or pollutants from the Asian monsoon anticyclone to mid and high latitudes of the Northern Hemisphere (Dethof et al., 1999; Garny and Randel, 2013). These air masses can be transported into the extratropical lower stratosphere where they are eventually mixed irreversibly with the surrounding stratospheric air (Dethof et al., 1999; Garny and Randel, 2013) and thus affect the chemical and radiative balance of the extra-tropical UTLS.

In this paper, we show that fast transport from boundary emissions from Southeast Asia has the potential to affect the chemical composition of the lowermost stratosphere over Northern Europe. We focus on the question how transport pathways and time scales from surface emissions from Southeast Asia are influenced by the Asian monsoon circulation and its interaction with tropospheric weather systems.

We use in situ measurements obtained during the TACTS (Transport and Composition in the Upper Troposphere and Lowermost Stratosphere) aircraft campaign 2012 and Lagrangian backward trajectories calculated with the trajectory module of the Chemical Lagrangian Model of the Stratosphere (CLaMS) (e.g., McKenna et al., 2002a, b; Konopka et al., 2010, and references therein). Pure trajectory models represent the advective transport by the resolved flow using three-dimensional winds from

ACPD
14, 18461–18497, 2014

meteorological data sets and are therefore useful for investigating of the origin of air masses, in particular in the region of the Asian monsoon anticyclone (Dethof et al., 1999; Chen et al., 2012; Bergman et al., 2013). The paper is organised as follows: Sect. 2 describes the measurements and Sect. 3 the trajectory calculations. In Sect. 4, the interaction of tropospheric weather systems, in particular of typhoons, with the Asian monsoon anticyclone and the resulting impact on the behaviour of the backward trajectories is discussed. A short summary and conclusion are given in Sect. 5.

2 Measurements of enhanced tropospheric trace gases in the stratosphere over Northern Europe

We use in situ measurements obtained during the TACTS aircraft campaign in August and September 2012. The TACTS campaign was designed to study Transport and Composition in the Upper Troposphere and Lowermost Stratosphere. It was conducted jointly with the ESMVal (Earth System Model Validation) measurement campaign. Both TACTS and ESMVal were performed using the German High Altitude and LOng Range Research Aircraft HALO, a Gulfstream V.

Here, we focus on the last research flight performed during TACTS/ESMVal on 26 September 2012 based out of Special Airport Oberpfaffenhofen (near Munich, 48° N 11° E), Germany. The flightpath is shown in Fig. 1 in conjunction with PV at 375 K potential temperature. The flight was flown roughly to the west to the British Isles, then to the north to the Atlantic Ocean, thereafter to the east towards Scandinavia. A closed loop flight track (hexagon) was conducted over Norway to test the capability of the newly developed Gimballed Limb Observer for Radiance Imaging of the Atmosphere (GLORIA) to sound the atmosphere tomographically (Kaufmann et al., 2014; Riese et al., 2014). Thereafter, a flight pattern with a steep descent to the lower troposphere and directly afterwards a step ascent back to the stratosphere (referred to as “dive”) was flown inside the hexagon. The research flight ended in Oberpfaffenhofen.

In this work, measurements of the following in situ instruments are used:

ACPD
14, 18461–18497, 2014

– The measurements of CO and CH_4 during TACTS/ESMVal were made with the TRIHOP instrument, which is an updated version of the three-channel tunable diode laser instrument for atmospheric research (TRISTAR), which has been used during the SPURT[1] project (Hoor et al., 2004; Engel et al., 2006). TRIHOP achieves a precision of 0.9 ppbv for CO and 5 ppbv for CH_4, respectively, for 1.5 s integration time. We estimate the reproducibility during the flights was 2.3 ppbv for CO and 15 ppbv for CH_4, respectively, without any corrections applied.

– The water measurements on board the HALO aircraft were obtained by the Fast In-situ Stratospheric Hygrometer (FISH) which is based on the Lyman-α photofragment fluorescence technique. Instrument and calibration procedure are described in Zöger et al. (1999). The FISH inlet is mounted forward-facing thus measuring total water, i.e. the sum of gas-phase water and water in ice particles. The procedure to correct the data for oversampling of ice particles in the forward-facing inlet is discussed in Schiller et al. (2008).

– A light-weight (14.5 kg) instrument (named FAIRO) for measuring ozone (O_3) with high accuracy (2 %) and high time resolution (10 Hz) was developed for the use on board HALO. It combines a dual-beam UV photometer with an UV-LED as light source and a dry chemiluminescence detector (Zahn et al., 2012). The performance of FAIRO was excellent during all 13 flights during TACTS/ESMVAL.

– Potential temperature is deduced from the Basic Halo Measurement and Sensor System (BAHAMAS) which yield basic meteorological and avionic data of HALO.

Figure 2 shows potential temperature (top, black dots) at the measurement location, CO and O_3 (middle), and CH_4 and H_2O (bottom) along the flightpath of the flight on 26 September 2012. In the first half of the flight at altitudes between 370 K and 380 K potential temperature, enhanced concentrations of tropospheric trace gases CO, CH_4, and H_2O were measured in the lowermost stratosphere and also reduced values of

[1]SPURenstofftransport in der Tropopausenregion (SPURT)

ACPD
14, 18461–18497, 2014

the stratospheric trace gas O_3. In Fig. 2, the time period from 09:05 UTC to 10:17 UTC with enhanced tropospheric trace gases and reduced ozone, respectively, is shaded in grey. Strong gradients are found in tracer measurements (at the beginning and the end of this time period) at the same level of potential temperature indicating that air masses were sampled with strongly different origin compared to the background air probed in this part of the flight. The region showing the enhanced tropospheric trace gases is referred to as "region of interest". The region of interest is located at the northwestern flank of the flight path over the Atlantic Ocean as shown in Fig. 1 (shown as white line in the flightpath). The potential vorticity (PV) at 375 K potential temperature indicates that in the region of interest and in the hexagon lower values of PV (7.3–8.0 PVU, yellow in Fig. 1) occur than in the stratospheric background, corroborating that these air masses have a different origin, that is more tropospheric, compared to the background. This is also evident in the Fig. 2, where within the flight part shortly before the dive (≈ 13:00 UTC) conducted within the hexagon enhanced CO, CH_4, and H_2O and reduced O_3 was measured simultaneously. Between 08:05 UTC and 08:23 UTC a tropospheric signal is also evident in the observations (see Fig. 2) measured over the British Isles (Fig. 1). However, in the region of interest the measured signatures are most pronounced and therefore we focus here on that part of the flight.

3 Results of backward trajectory calculations

To study the origin of air in the region of interest (highlighted in grey in Fig. 2) 40 day backward trajectories are calculated along the flightpath using wind data from the ERA-Interim re-analysis (Dee et al., 2011) (with a horizontal resolution of $1^\circ \times 1^\circ$) provided by the European Centre for Medium-Range Weather Forecasts (ECMWF). For trajectory calculations, the trajectory module of the Chemical Lagrangian Model of the Stratosphere (CLaMS) (McKenna et al., 2002b; Konopka et al., 2012, and references therein) is used. Trajectory calculations with CLaMS can be performed in both the diabatic mode and the kinematic mode, i.e. using potential temperature or pressure, respectively, as

ACPD
14, 18461–18497, 2014

the vertical coordinate (Ploeger et al., 2010). Here, the diabatic approach is applied. This implies using the diabatic heating rate (with contributions from radiative heating including the effects of clouds, latent heat release, mixing and diffusion) as vertical velocity. The transport is simulated with vertical velocities from the diabatic heating rate in the UTLS (< 300 hPa) and using a pressure based hybrid vertical coordinate in the troposphere (> 300 hPa) (Pommrich et al., 2014).

40 day backward trajectories starting at the observation along the flight path (every 10 s) on 26 September 2012 and ending at the origin of the air masses in the past (17 August 2012) are calculated. The potential temperature at the air mass origin (Θ_{org}) gives information about the vertical transport of the air mass along the trajectory. In Fig. 2 (top), the potential temperature at the air mass origin (Θ_{org}) is shown as red dots. Most Θ_{org} values lie above or at the same level of potential temperature as during the flight, consistent with the descent of air masses in the lower stratosphere of the Northern Hemisphere. However, in the region of interest some of the air masses originate at much lower levels of potential temperature, namely between 295 K and 360 K.

In Fig. 3, two Θ_{org} intervals, 295–320 K (left) and 320–360 K (right), are shown colour-coded by potential temperature (top) and by days reversed from 26 September 2012 (middle). Further, the geographical air mass origin (bottom, red dots in embedded map) and potential temperature vs. time along the 40 day backward trajectories (bottom) colour-coded by latitude are shown.

All air parcels with Θ_{org} below 360 K are affected by air masses originating from the Asian monsoon anticyclone (Fig. 3, top). The air parcels are separated from the Asian monsoon circulation in the region over Japan, East China, and Southeast Siberia approximately 8–14 days before they were sampled during the flight on 26 September 2012 (Fig. 3, middle).

Air masses with Θ_{org} lower than 320 K originate at much lower levels of potential temperature and are lifted between 35 and 40 days before the flight over the West Pacific (Fig. 3, left middle). Afterwards, they move first anti-clockwise at the edge of

ACPD
14, 18461–18497, 2014

the anticyclone (at ≈ 365 K), then turn over Japan before they become entrained into the Asian monsoon circulation and then move further around the Asian monsoon (left middle). For Θ_{org} between 320 K and 360 K, some of the air masses intrude directly into the anticyclone and move clockwise round the Asian monsoon at the edge of the anticyclonic circulation. Other trajectories perform first a loop over the West Pacific ocean (right middle).

Some of the air parcels with Θ_{org} lower than 320 K show a very rapid uplift between 23 and 25 August with a maximum ascent rate of 41 K day^{-1} (= 523 hPa day^{-1}) and originate in Southeast Asia (left bottom). Air parcels with Θ_{org} between 320 K and 360 K are characterised by rapid uplift up to 13 K day^{-1} (= 139 hPa day^{-1}) between 18 and 24 August and originate in the West Pacific (northern or western of Philippines) or from northern of India (right bottom). An overview about maximum and mean vertical velocities is given in Table 1.

In the following we discuss also transport pathways of air masses originate in intervals for Θ_{org} between 360–370 K, 370–380 K, and 380–420 K. Related figures are not shown here, but are available as an electronic supplement of this paper.

Most air masses originating at Θ_{org} values between 360 K and 370 K experienced a moderately rapid uplift with mean values of about 2 K day^{-1} (= 22 hPa day^{-1}) roughly in the region of the Asian monsoon anticyclone. Most of these air masses originate in North Africa, South Asia, and in the West Pacific. The trajectories are separated from the anticyclone approximately 8–14 days before the flight on 26 September 2012, and therefore transport air masses from inside the Asian monsoon anticyclone to Northern Europe.

At levels above, for Θ_{org} between 370 K and 380 K, the trajectories are affected by both the Asian monsoon anticyclone and the subtropical westerly jet. The moderate uplift along the trajectories is 1 K day^{-1} (= 16 hPa day^{-1}) in the mean. The majority of air masses originate in regions around the Asian monsoon anticyclone and in Central America. In the latter case, the trajectories are most likely affected by the North American monsoon.

ACPD
14, 18461–18497, 2014

Most air masses that originate at Θ_{org} between 380 K and 420 K are dominated by the global circulation patterns with a descent of air masses in the Northern Hemisphere lower stratosphere. These trajectories do not circulate around the Asian monsoon anticyclone (except for two trajectories) and the air mass origins are spread out in the entire Northern Hemisphere, excluding regions affected by the Asian monsoon anticyclone such as South Asia or parts of North Africa. Our findings inferred from backward trajectory calculations are summarised in Table 1.

Our trajectory calculations suggest that potential boundary emissions from Southeast Asia and the West Pacific are rapidly uplifted and are transported within approximately 5 weeks to Northern Europe. The air mass origins are not found in surface regions located closed to the core of the Asian monsoon such as North India, South India or East China. This suggests that in our study possible boundary emissions from these regions need a longer time period of upward transport within the Asian monsoon anticyclone to reach the lowermost stratosphere over Northern Europe.

In this work, we focus on the region of interest (cf. Sect. 2), however also in other parts of the flight enhanced tropospheric signals in tracers and reduced ozone are measured between 08:05 UTC and 08:23 UTC and along the hexagon before the dive. The latter signal is also caused by transport of air masses from lower levels of potential temperature as evident in 40 day backward trajectories (Fig. 3, top). The tropospheric signal between 08:05 UTC and 08:23 UTC is not present in 40 day backward trajectories, but in 50 day backward trajectories to a small extend. The trajectories from lower levels originate in South Asia, Northwest America and over the Atlantic ocean.

4 Interaction between the Asian monsoon anticyclone and other tropospheric weather systems

To understand the behaviour of the backward trajectories presented in the previous section, the meteorology of the Asian monsoon area will be analysed based on ERA-Interim re-analysis data (Dee et al., 2011). In August 2012, the Asian monsoon anticy-

ACPD
14, 18461–18497, 2014

clone was well established over Southern Asia and the Middle East. The Asian monsoon anticyclone is characterised by low PV values, indicating that it consists mainly of air masses of tropospheric origin. To the north the Asian monsoon anticyclone is connected to the subtropical jet, to the south the equatorial westward flow is adjacent. The Asian monsoon anticyclone extends over a height range from 400 hPa or 340 K upward well into the lowermost stratosphere.

During August and September 2012 several tropical cyclones had impact on meteorological conditions in the vicinity of the Asian monsoon anticyclone. Further, during September 2012 the subtropical jet over Asia was disturbed by strong Rossby waves triggered by low pressure systems travelling with the Arctic jet. The interaction between these disturbances and the Asian monsoon anticyclone is discussed in the next sections.

4.1 Very rapid uplift in tropical cyclones in August 2012

In the northwestern Pacific region, tropical cyclones (typhoons) are observed at all times of the year, with storm activity peaking in late northern summer (e.g., Emanuel, 2003). In August and September 2012, several major typhoons of the category 4 or 5 according to the Saffir–Simpson hurricane wind scale (SSHWS) occurred in northwestern Pacific region.

Between 18 and 20 August 2012, the typhoon Tembin (named Igme by the Philippine Atmospheric, Geophysical and Astronomical Services Administration PAGASA) grew from a tropical depression to a category 4 typhoon southeast of Taiwan[2]. Only a few days later the tropical typhoon Bolaven (PAGASA name Julian) formed east of the Philippines and moved northwest towards Taiwan. Bolaven was also classified as

[2] see e.g., http://www.nasa.gov/mission_pages/hurricanes/archives/2012/h2012_Tembin.html

ACPD
14, 18461–18497, 2014

a class 4 typhoon[3]. After having made landfall twice in Taiwan, Tembin started to interact with Bolaven on 25 August, forcing it to move further to the north, where it made landfall in Korea on 28 August. Two days later, Tembin made landfall in Korea as well.

Figure 4 (top) shows the geographical position of the typhoons Tembin and Bolaven on 24 August 2012. Tembin was located over Taiwan, Bolaven further to the east over the Philippine Sea, being much stronger than Tembin at that time. The position of Bolaven coincides in time and space with the very rapid uplift of air masses evident in the trajectory calculations for Θ_{org} between 295 K and 320 K on 23/24 August 2012 (see Fig. 3, bottom).

Figure 4 (bottom) shows that both typhoons lifted air masses rapidly from the lower troposphere up to the tropopause region. The maximum updraft occurs at the eyewall, a ring of very deep convective clouds extending from the outer edge of the eye outward another 20–50 km (Emanuel, 2003). Maximum vertical uplift up to 300 hPa within 6 h (0.014 hPa s^{-1}) is found at around 135° E at the eastern flank of Bolaven. This very rapid vertical transport is consistent with upward motion calculated along the 40 day backward trajectories of up to 276 hPa/6 h (see Table 1).

Bolaven moved northward during the next 4 days until it made landfall in Korea. This motion is also visible in the 40 day backward trajectories for Θ_{org} between 295 K and 310 K. Along the trajectories the air parcels move first cyclonically around the typhoon, before they move northward and enter the outer edge of the anticyclonic flow of the Asian monsoon anticyclone over Korea at ≈ 370 K (see Fig. 3 left middle panel).

In summary, our trajectory calculations show that typhoons in the northern West Pacific have the potential to very rapidly uplift air masses from the sea surface up to altitudes of the Asian monsoon anticyclonic circulation within 1 to 2 days. Balloon measurements of water vapour and ozone in the Asian monsoon anticyclone launched in Kunming (China) in August 2009 show likewise a very rapid uplift of boundary sources associated with the typhoon Morakot and afterwards injection of these air masses in

[3]see e.g., http://www.nasa.gov/mission_pages/hurricanes/archives/2012/h2012_Bolaven.html

ACPD
14, 18461–18497, 2014

the Asian monsoon anticyclone (Munchak et al., 2010). These measurements support the results of our trajectory calculations for September 2012 showing that rapid uplift by typhoons in the West Pacific may transport air parcels from the boundary layer directly in the outer edge of the Asian monsoon anticyclone.

4.2 Asian monsoon anticyclone and eddy shedding in September 2012

In August 2012, the Asian monsoon anticyclone was well established over Southern Asia and the Middle East. During both August and September the Asian monsoon anticyclone was influenced by strong Rossby waves and by several tropical cyclones.

A time sequence of PV fields at 370 K potential temperature over Asia from 9 until 20 September 2012 is shown in Fig. 5 (colours) highlighting the fine-scale structure of PV in the anticyclone and the eastward propagation of filaments with low PV values at its northeastern flank (showing PV values < 5 PVU). In addition, the horizontal velocity (white arrows) characterising spatial and temporal evolution of the flow in the Asian monsoon anticyclone are shown.

On 9 September 2012, the Asian monsoon anticyclone is located over South Asia and Northeast Africa (Fig. 5). At the northeastern flank of the anticyclone filaments with PV values lower than 5 PVU evolve between 10–14 September. The filament with low PV is extruded eastward along the subtropical westerly jet. A separation of the filament from the Asian monsoon circulation occurred and a small anticyclonic system developed during 15–16 September 2012. Thereafter, the secondary small anticyclone is elongated, moves westward and merges with an other newly formed filament on the eastern flank of the Asian monsoon with low PV values close to Japan on 17/18 September. On 20 September, again a secondary anticyclone, larger than the secondary anticyclone from 15/16 September, is separated from the Asian monsoon anticyclone and carries air with low PV to the Pacific Ocean. Finally, the low PV air moves further eastwards along the subtropical jet across the extratropical tropopause to Northern Europe and dissipates with time in the Northern Hemisphere lowermost stratosphere. The process of peeling off secondary anticyclonic structures is called

ACPD
14, 18461–18497, 2014

eddy shedding event and occurs a few times each summer (Dethof et al., 1999; Hsu and Plumb, 2001; Popovic and Plumb, 2001) (cf. Sect. 1). Figure 5 shows that both the Asian monsoon anticyclone and the secondary eastward propagating anticyclones are characterised by low PV values, indicating that it consists mainly of air masses of tropospheric origin.

The general behaviour of 40 day backward trajectories shown in Fig. 3 can be explained by the temporal evolution of the Asian monsoon anticyclone. Nearly all trajectories below a Θ_{org} of 380 K are affected by the eddy shedding event on 20 September 2012 or by the separation of filaments with low PV values at the northeastern flank of the anticyclone.

4.3 Reasons for eastward eddy shedding and intensification by a super typhoon

Dethof et al. (1999) suggested that mid-latitude synoptic disturbances occasionally interact with the Asian monsoon anticyclone and might pull filaments of tropospheric air from its northern flank. This process is referred to as eastward eddy shedding (Hsu and Plumb, 2001; Popovic and Plumb, 2001). Such a situation occurred in September 2012. The subtropical jet was disturbed by strong Rossby waves triggered by low pressure systems travelling with the Arctic jet. The interaction between these disturbances and the subtropical jet can lead to baroclinic instabilities and eddy shedding (e. g. Orlanski and Sheldon, 1995).

Under such circumstances, tropospheric air masses from the the Asian monsoon anticyclone are separated within a secondary anticyclone which is still a tropospheric feature as indicated by low PV values. The transport of air masses into the lowermost stratosphere occurs afterwards. In contrast, tropospheric intrusions transport directly quasi-isentropically air masses from the tropical tropopause layer (TTL) into the extratropical lowermost stratosphere where the air masses are mixed irreversibly (e.g., Vogel et al., 2011b). This can be caused by Rossby wave breaking events along the subtropical jet (e.g., Homeyer et al., 2011).

ACPD
14, 18461–18497, 2014

Moreover, the eddy shedding event of 20 September 2012 was intensified by interaction between the baroclinic waves and a super typhoon (class 5), leading to a weakening of the Asian monsoon anticyclone in its intensity and coherent horizontal structure. Riemer and Jones (2013) show that the impact of a tropical cyclone on the Rossby wave can be quantified as a source of wave activity for the upper-level wave and is sensitive to the phasing between the tropical cyclone and the wave. The interaction with the tropical cyclone can in general initiate wave breaking and, in case of the Asian monsoon anticyclone, lead to the shedding of secondary anticyclones from the main anticyclone.

On 10 September 2012, the super typhoon Sanba (PAGASA name Karen) formed as a tropical depression east of the Philippines and started moving northward. Three days later the storm system underwent a strong intensification and evolved into the strongest typhoon (class 5) during 2012 in the western Pacific region[4] (see Fig. 5). It made landfall on 17 September in South Korea and changed into an extratropical cyclone afterwards (see Fig. 5).

A trough evolved upstream of the Himalayan plateau on 16 September 2012. This perturbation pushed the circulation of the Asian monsoon anticyclone equatorwards and led to a split of the anticyclone in a western part centred over the Arabian peninsula and an eastern part over northern India. The western part weakened during the following days. At this stage the super typhoon Sanba approached the trough off the coast of South Korea (see Fig. 5). The subsequent interaction between the tropical typhoon and the baroclinic wave led to a strong amplification of the system. The typhoon acted as a source for eddy kinetic energy, leading to a strengthening of the meridional wind. The mid-latitude synoptic disturbances yield eastward eddy shedding strengthened by the super typhoon Sanba (see Fig. 5).

In summary, our trajectory calculations show that typhoons in the northern west Pacific have the potential to very rapidly lift air masses from the sea surface to the edge

[4] see e.g., http://www.nasa.gov/mission_pages/hurricanes/archives/2012/h2012_Sanba.html

ACPD
14, 18461–18497, 2014

of the Asian monsoon anticyclone within 1 to 2 days. In combination with the monsoon anticyclone and eastward eddy shedding events, this constitutes a new rapid transport pathway of surface emissions form the West Pacific to Northern Europe. In our study, the minimum transport times from surface to the lowermost stratosphere over Northern Europe are approximately 5 weeks. Moistening of the stratosphere is an important driver of climate change, therefore the role of this new rapid transport pathway in moistening of the extratropical lower stratosphere during summer needs further investigation.

Moreover, in the last 30 years a poleward migration occurred of the latitude where tropical cyclones achieve their lifetime-maximum intensity (Kossin et al., 2014). If this environmental change continues, more tropical cyclones migrate polwards to the northeastern flank of the Asian monsoon anticyclone. Therefore, the frequency of occurrence of both the direct injections of polluted boundary layer air masses by very rapid uplift in typhoons into the Asian monsoon anticyclone and the strength of eastward eddy shedding events could increase.

5 Conclusions

On 26 September 2012, a filament with enhanced tropospheric trace gases such as CH_4, CO, and H_2O and reduced stratospheric O_3 was measured over Northern Europe in the extratropical lowermost stratosphere during a flight on board the German Research Aircraft HALO during the TACTS campaign. Trajectory calculations show that these air masses originate in Southeast Asia and are affected by the Asian monsoon anticyclone. Based on our analysis of these observations and the associated trajectory calculations, we propose a new rapid transport pathway of approximately 5 weeks from the boundary layer sources in Southeast Asia to the location of the measurement in the lowermost stratosphere over Northern Europe.

Our findings show that air originating in the polluted boundary layer in South East Asia can be very rapidly lifted within 1–2 days by Pacific typhoons into air masses

ACPD
14, 18461–18497, 2014

circulating around the Asian monsoon anticyclone (at ≈ 365 K potential temperature). Similar timescales are found for deep convection overshooting in this region (Chen et al., 2012) or in convective transport in the West African tropics (e.g., Fierli et al., 2011). Therefore, our findings confirm evidence from previous studies that at the eastern side of the anticyclone tropospheric air masses are lifted and trapped in the anticyclone (Li et al., 2005) or can be injected by convection into the stratosphere (Rosenlof et al., 1997; Park et al., 2007, 2008; Chen et al., 2012). Moreover, boundary emissions from the core of Asian monsoon anticyclone are not found in 40 day backward trajectories, suggesting that transport from boundary emissions from India and China through the Asian monsoon anticyclone is slower.

In Fig. 6, selected 40 day backward trajectories representing characteristic pathways with different vertical velocities (cf. Table 1) are shown as function of potential temperature and longitude summarising our results. The figure illustrates different transport pathways of air masses with different origin to the location of the measurement over Northern Europe. The observed air masses in the region of interest are a mixture of air masses with distinct origins in different fractions (cf. Table 1). The combination of very rapid uplift by a typhoon and eastward eddy shedding from the Asian monsoon anticyclone yield fast transport (≈ 5 weeks) from Southeast Asia boundary layer sources to Northern Europe (2 % of all trajectories, red). Some of the 40 day backward trajectories originate in the West Pacific troposphere (3 %, blue) or within the Asian monsoon anticyclone over South Asia/North Africa (12 %, green). Air masses that originate in the UTLS at altitudes between 370 K and 380 K potential temperature are mainly from the edge of the Asian monsoon anticyclone (22 %, yellow). Most air parcels originate at higher altitudes between 380 K and 420 K. These air parcels come from the entire Northern Hemisphere, with the exception of the region of the Asian monsoon anticyclone (61 %, grey).

Further, our calculations show that after the injection into the anticyclonic circulation, the air masses circulate clockwise, in an upward spiral, at the edge of the Asian monsoon anticyclone around the core of the anticyclone and do not enter the core of the

ACPD
14, 18461–18497, 2014

anticyclone itself. In addition to the upward transport within the Asian monsoon connecting surface air with enhanced pollution to the lower stratosphere (e.g., Park et al., 2009; Randel et al., 2010; Chen et al., 2012; Bergman et al., 2013), the injection into the outer edge of the anticyclone and subsequent clockwise circulation around the core of the anticyclone is an additional pathway of air mass transport from the Asian monsoon anticyclone to the lowermost stratosphere. During the Nabro volcanic eruption in 2011, direct injections in the upper troposphere at the southwest flank of the Asian monsoon anticyclone (over Northwest Africa) have been observed by satellite observations by the Michelson Interferometer for Passive Atmospheric Sounding (MIPAS) (Griessbach et al., 2013). The MIPAS observations also show clockwise transport of air masses injected directly at the southwest flank in the outer edge of the Asian monsoon anticyclone. This support our findings about the clockwise transport of air masses injected directly at the east flank by typhoons around the core of the Asian monsoon anticyclone.

Our analysis shows that an eastward eddy shedding event occurred mid of September 2012. The subtropical jet was disturbed by strong Rossby waves triggered by low pressure systems travelling with the Arctic jet. The interaction between these disturbances and the subtropical jet led to the peeling off of secondary anticyclonic structures from the Asian monsoon anticyclone. In addition, this eddy shedding event was intensified by the interaction with the super typhoon Sanba.

The backward trajectories show that the transport time of water vapour and pollutants from the Asian monsoon anticyclone to Northern Europe caused by eddy shedding events and transport along the subtropical jet is about 8–14 days in the case study discussed here. Thereafter, the trajectories travel further northeastwards along the subtropical jet to the Pacific Ocean and finally to Northern Europe. In our study, moisture and pollution are transported very fast within up to 5 weeks from the lower troposphere in Southeast Asia to the lowermost stratosphere over Northern Europe caused by the combination of very rapid uplift by a typhoon and eastward eddy shedding from the Asian monsoon anticyclone. This rapid transport pathway into the lowermost strato-

ACPD
14, 18461–18497, 2014

sphere is for short-lived substances (e.g. bromine-containing short-lived source gases) of particular importance. Eddy shedding events have the potential for long-range transport of enhanced concentrations of boundary layer sources such as water vapour and pollutants from Southeast Asia to mid and high latitudes of the Northern Hemisphere lowermost stratosphere.

The Supplement related to this article is available online at doi:10.5194/acpd-14-18461-2014-supplement.

Acknowledgements. We sincerely thank Andreas Engel and Harald Bönisch (University Frankfurt) for coordinating the TACTS campaign and the HALO crew and pilots. The authors gratefully acknowledge Paul Konopka and Felix Plöger for helpful discussions about the Asian monsoon circulation and Laura Pan for discussions about the balloon observations in China associated with the strong uplift in typhoons. We thank the European Centre of Medium-Range Weather Forcasts (ECMWF) for providing meteorological analyses and the ERA-Interim reanalysis data. Our activities, flight planning and forecasts were partly founded by the German Science Foundation (Deutsche Forschungsgemeinschaft, DFG) under the DFG project LASSO (HALO-SPP 1294/GR 3786).

The service charges for this open access publication have been covered by a Research Centre of the Helmholtz Association.

References

Bannister, R. N., O'Neill, A., Gregory, A. R., and Nissen, K. M.: The role of the south-east Asian monsoon and other seasonal features in creating the "tape-recorder" signal in the Unified Model, Q. J. Roy. Meteor. Soc., 130, 1531–1554, 2004. 18464

ACPD
14, 18461–18497, 2014

Bergman, J. W., Fierli, F., Jensen, E. J., Honomichl, S., and Pan, L. L.: Boundary layer sources for the Asian anticyclone: regional contributions to a vertical conduit, J. Geophys. Res., 118, 2560–2575, doi:10.1002/jgrd.50142, 2013. 18464, 18466, 18479

Bourassa, A. E., Robock, A., Randel, W. J., Deshler, T., Rieger, L. A., Lloyd, N. D., Llewellyn, E. J. T., and Degenstein, D. A.: Large volcanic aerosol load in the stratosphere linked to Asian monsoon transport, Science, 337, 78–81, doi:10.1126/science.1219371, 2012. 18464

Chen, B., Xu, X. D., Yang, S., and Zhao, T. L.: Climatological perspectives of air transport from atmospheric boundary layer to tropopause layer over Asian monsoon regions during boreal summer inferred from Lagrangian approach, Atmos. Chem. Phys., 12, 5827–5839, doi:10.5194/acp-12-5827-2012, 2012. 18464, 18466, 18478, 18479

Dee, D. P., Uppala, S. M., Simmons, A. J., Berrisford, P., Poli, P., Kobayashi, S., Andrae, U., Balmaseda, M. A., Balsamo, G., Bauer, P., Bechtold, P., Beljaars, A. C. M., van de Berg, L., Bidlot, J., Bormann, N., Delsol, C., Dragani, R., Fuentes, M., Geer, A. J., Haimberger, L., Healy, S. B., Hersbach, H., Holm, E. V., Isaksen, L., Kallberg, P., Koehler, M., Matricardi, M., McNally, A. P., Monge-Sanz, B. M., Morcrette, J. J., Park, B.-K., Peubey, C., de Rosnay, P., Tavolato, C., Thepaut, J. N., and Vitart, F.: The ERA-Interim reanalysis: configuration and performance of the data assimilation system, Q. J. Roy. Meteor. Soc., 137, 553–597, doi:10.1002/qj.828, 2011. 18468, 18471

Dethof, A., O'Neill, A., Slingo, J. M., and Smit, H. G. J.: A mechanism for moistening the lower stratosphere involving the Asian summer monsoon, Q. J. Roy. Meteor. Soc., 556, 1079–1106, 1999. 18464, 18465, 18466, 18475

Dunkerton, T. J.: Evidence of meridional motion in the summer lower stratosphere adjacent to monsoon regions, J. Geophys. Res., 100, 16675–16688, 1995. 18462

Dvortsov, V. L. and Solomon, S.: Response of the stratospheric temperatures and ozone to past and future increases in stratospheric humidity, J. Geophys. Res., 106, 7505–7514, 2001. 18463

Emanuel, K.: Tropical cyclons, Annu. Rev. Earth Pl. Sc., 3, 75–104, 2003. 18472, 18473

Engel, A., Bönisch, H., Brunner, D., Fischer, H., Franke, H., Günther, G., Gurk, C., Hegglin, M., Hoor, P., Königstedt, R., Krebsbach, M., Maser, R., Parchatka, U., Peter, T., Schell, D., Schiller, C., Schmidt, U., Spelten, N., Szabo, T., Weers, U., Wernli, H., Wetter, T., and Wirth, V.: Highly resolved observations of trace gases in the lowermost stratosphere and

ACPD
14, 18461–18497, 2014

upper troposphere from the Spurt project: an overview, Atmos. Chem. Phys., 6, 283–301, doi:10.5194/acp-6-283-2006, 2006. 18467
Fierli, F., Orlandi, E., Law, K. S., Cagnazzo, C., Cairo, F., Schiller, C., Borrmann, S., Di Donfrancesco, G., Ravegnani, F., and Volk, C. M.: Impact of deep convection in the tropical tropopause layer in West Africa: in-situ observations and mesoscale modelling, Atmos. Chem. Phys., 11, 201–214, doi:10.5194/acp-11-201-2011, 2011. 18478
Forster, P. and Shine, K. P.: Stratospheric water vapour change as possible contributor to observed stratospheric cooling, Geophys. Res. Lett., 26, 3309–3312, doi:10.1029/1999GL010487, 1999. 18463
Forster, P. and Shine, K. P.: Assessing the climate impact of trends in stratospheric water vapor, Geophys. Res. Lett., 29, 10-1–10-4 doi:10.1029/2001GL013909, 2002. 18463
Garny, H. and Randel, W. J.: Dynamic variability of the Asian monsoon anticyclone observed in potential vorticity and correlations with tracer distributions, J. Geophys. Res., 118, 13421–13433, doi:10.1002/2013JD020908, 2013. 18465
Gettelman, A., Kinnison, D., Dunkerton, T. J., and Brasseur, G. P.: Impact of monsoon circulations on the upper troposphere and lower stratosphere, J. Geophys. Res., 109, D22101, doi:10.1029/2004JD004878, 2004. 18464
Griessbach, S., Hoffmann, L., Spang, R., von Hobe, M., Müller, R., and Riese, M.: MIPAS Volcanic Sulfate Aerosol Observations of the Nabro Eruption, in: Stratospheric Sulfur and its Role in Climate (SSiRC), Atlanta, Georgia, USA, October 2013, SPARC, available at: http://www.sparc-ssirc.org/downloads/Griessbach.pdf, 2013. 18479
Highwood, E. J. and Hoskins, B. J.: The tropical tropopause, Q. J. Roy. Meteor. Soc., 124, 1579–1604, 1998. 18462
Holton, J. R., Haynes, P., McIntyre, M. E., Douglass, A. R., Rood, R. B., and Pfister, L.: Stratosphere–troposphere exchange, Rev. Geophys., 33, 403–439, 1995. 18464
Homeyer, C. R., Bowman, K. P., Pan, L. L., Atlas, E. L., Gao, R.-S., and Campos, T. L.: Dynamical and chemical characteristics of tropospheric intrusions observed during START08, J. Geophys. Res., 116, D06111, doi:10.1029/2010JD015098, 2011. 18475
Hoor, P., Gurk, C., Brunner, D., Hegglin, M. I., Wernli, H., and Fischer, H.: Seasonality and extent of extratropical TST derived from in-situ CO measurements during SPURT, Atmos. Chem. Phys., 4, 1427–1442, doi:10.5194/acp-4-1427-2004, 2004. 18467
Hsu, C. J. and Plumb, R. A.: Nonaxisymmetric thermally driven circulations and upper-tropospheric monsoon dynamics, J. Atmos. Sci., 57, 1255–1276, 2001. 18465, 18475

ACPD
14, 18461–18497, 2014

Huang, Y., Zhang, W., Zheng, X., Li, J., and Yu, Y.: Modeling methane emission from rice paddies with various agricultural practices, J. Geophys. Res., 109, D8113, doi:10.1029/2003JD004401, 2004. 18463

Hurst, D. F., Oltmans, S. J., Vömel, H., Rosenlof, K. H., Davis, S. M., Ray, E. A., Hall, E. G., and Jordan, A. F.: Stratospheric water vapor trends over Boulder, Colorado: analysis of the 30 year Boulder record, J. Geophys. Res., 116, D02306, doi:10.1029/2010JD015065, 2011. 18463

Jackson, D. R., Driscoll, S. J., Highwood, E. J., Harries, J. E., and Russell III, J. M.: Troposphere to stratosphere transport at low latitudes as studies using HALOE observations of water vapor 1992–1997, Q. J. Roy. Meteor. Soc., 124, 169–192, 1998. 18463

Kaufmann, M., Blank, J., Guggenmoser, T., Ungermann, J., Engel, A., Ern, M., Friedl-Vallon, F., Gerber, D.„ Grooß, J. U., Günther, G., Höpfner, M., Kleinert, A., Latzko, T., Maucher, G., Neubert, T., Nordmeyer, H., Oelhaf, H., Olschewski, F., Orphal, J., Preusse, P., Schlager, H., Schneider, H., Schuettemeyer, D., Stroh, F., Sumińska-Ebersoldt, O., Vogel, B., Volk, M., Wintel, J., Woiwode, W., and Riese, M.: Retrieval of three-dimensional small scale structures in upper tropospheric/lower stratospheric composition as measured by GLORIA, Atmos. Meas. Tech. Discuss., 7, 4229–4274, doi:10.5194/amtd-7-4229-2014, 2014. 18466

Khalil, M. A. K., Rasmussen, R. A., Shearer, M. J., Dalluge, R. W., Ren, L. X., and Duan, C. L.: Measurements of methane emissions from rice fields in China, J. Geophys. Res., 103, 25181–25210, 1998. 18463

Kirk-Davidoff, D. B., Hintsa, E. J., Anderson, J. G., and Keith, D. W.: The effect of climate change on ozone depletion through changes in stratospheric water vapour, Nature, 402, 399–401, doi:10.1038/46521, 1999. 18463

Konopka, P., Grooß, J.-U., Günther, G., Ploeger, F., Pommrich, R., Müller, R., and Livesey, N.: Annual cycle of ozone at and above the tropical tropopause: observations versus simulations with the Chemical Lagrangian Model of the Stratosphere (CLaMS), Atmos. Chem. Phys., 10, 121–132, doi:10.5194/acp-10-121-2010, 2010. 18464, 18465

Konopka, P., Ploeger, F., and Müller, R.: Entropy-based and static stability based Lagrangian model grids, in: Lagrangian Modeling of the Atmosphere, Geophysical Monograph Series, 200, AGU Chapman Conference on Advances in Lagrangian Modeling of the Atmosphere, Grindelwald, Switzerland, 9–14 October 2011, 99–109, 2012. 18468

ACPD
14, 18461–18497, 2014

Kossin, J. P., Emanuel, K. A., and Vecchi, G. A.: The poleward migration of the location of tropical cyclone maximum intensity, Nature, 509, 349–352, doi:10.1038/nature13278, 2014. 18477

Kunz, A., Müller, R., Homonnai, V., Jánosi, I., Hurst, D., Rap, A., Forster, P., Rohrer, F., Spelten, N., and Riese, M.: Extending water vapor trend observations over Boulder into the tropopause region: trend uncertainties and resulting radiative forcing, J. Geophys. Res., 118, 11269–11284, doi:10.1002/jgrd.50831, 2013. 18463

Li, Q., Jiang, J. H., Wu, D. L., Read, W. G., Livesey, N. J., Waters, J. W., Zhang, Y., Wang, B., Filipiak, M. J., Davis, C. P., Turquety, S., Wu, S., Park, R. J., Yantosca, R. M., and Jacob, D. J.: Convective outflow of South Asian pollution: a global CTM simulation compared with EOS MLS observations, Geophys. Res. Lett., 32, L14826, doi:10.1029/2005GL022762, 2005. 18463, 18464, 18478

Liu, Y., Wang, Y., Liu, X., Cai, Z., and Chance, K.: Tibetan middle tropospheric ozone minimum in June discovered from GOME observations, Geophys. Res. Lett., 36, L05814, doi:10.1029/2008GL037056, 2009. 18464

McKenna, D. S., Grooß, J.-U., Günther, G., Konopka, P., Müller, R., Carver, G., and Sasano, Y.: A new Chemical Lagrangian Model of the Stratosphere (CLaMS): 2. Formulation of chemistry scheme and initialization, J. Geophys. Res., 107, 4256, doi:10.1029/2000JD000113, 2002a. 18465

McKenna, D. S., Konopka, P., Grooß, J.-U., Günther, G., Müller, R., Spang, R., Offermann, D., and Orsolini, Y.: A new Chemical Lagrangian Model of the Stratosphere (CLaMS): 1. Formulation of advection and mixing, J. Geophys. Res., 107, 4309, doi:10.1029/2000JD000114, 2002b. 18465, 18468

Munchak, L., Fan, Q., Pan, L., Bian, J., and Bowman, K.: An analysis of transport pathways that contribute to water vapor and ozone profiles measured in the Asian monsoon anticyclone, in: Fall Meeting, Fall Meeting, 13–17 December 2010, AGU, San Francisco, A51B-0080, 2010. 18474

Orlanski, I. and Sheldon, J. P.: Stages in the energetics of baroclinic systems, Tellus A, 47, 605–628, 1995. 18475

Park, M., Randel, W. J., Kinnison, D. E., Garcia, R. R., and Choi, W.: Seasonal variation of methane, water vapor, and nitrogen oxides near the tropopause: Satellite observations and model simulations, J. Geophys. Res., 109, D03302, doi:10.1029/2003JD003706, 2004. 18463

ACPD
14, 18461–18497, 2014

Park, M., Randel, W. J., Gettleman, A., Massie, S. T., and Jiang, J. H.: Transport above the Asian summer monsoon anticyclone inferred from Aura Microwave Limb Sounder tracers, J. Geophys. Res., 112, D16309, doi:10.1029/2006JD008294, 2007. 18463, 18464, 18478

Park, M., Randel, W. J., Emmons, L. K., Bernath, P. F., Walker, K. A., and Boone, C. D.: Chemical isolation in the Asian monsoon anticyclone observed in Atmospheric Chemistry Experiment (ACE-FTS) data, Atmos. Chem. Phys., 8, 757–764, doi:10.5194/acp-8-757-2008, 2008. 18463, 18464, 18478

Park, M., Randel, W. J., Emmons, L. K., and Livesey, N. J.: Transport pathways of carbon monoxide in the Asian summer monsoon diagnosed from Model of Ozone and Related Tracers (MOZART), J. Geophys. Res., 114, D08303, doi:10.1029/2008JD010621, 2009. 18463, 18464, 18479

Ploeger, F., Konopka, P., Günther, G., Grooß, J.-U., and Müller, R.: Impact of the vertical velocity scheme on modeling transport across the tropical tropopause layer, J. Geophys. Res., 115, D03301, doi:10.1029/2009JD012023, 2010. 18469

Ploeger, F., Günther, G., Konopka, P., Fueglistaler, S., Müller, R., Hoppe, C., Kunz, A., Spang, R., Grooß, J.-U., and Riese, M.: Horizontal water vapor transport in the lower stratosphere from subtropics to high latitudes during boreal summer, J. Geophys. Res., 118, 8111–8127, doi:10.1002/jgrd.50636, 2013. 18463

Pommrich, R., Müller, R., Grooß, J.-U., Konopka, P., Ploeger, P., Vogel, B., Tao, M., Hoppe, C., Günther, G., Hoffmann, L., Pumphrey, H.-C., Viciani, S., D'Amato, F., Volk, M., Hoor, P., and Riese, M.: Tropical troposphere to stratosphere transport of carbon monoxide and long-lived trace species in the Chemical Lagrangian Model of the Stratosphere (CLaMS), Geosci. Model Dev., submitted, 2014. 18469

Popovic, J. M. and Plumb, R. A.: Eddy Shedding from the upper-tropospheric Asian monsoon anticyclone, J. Atmos. Sci., 58, 93–104, 2001. 18465, 18475

Randel, W. J. and Park, M.: Deep convective influence on the Asian summer monsoon anticyclone and associated tracer variability observed with Atmospheric Infrared Sounder (AIRS), J. Geophys. Res., 111, D12314, doi:10.1029/2005JD006490, 2006. 18462, 18463, 18464

Randel, W. J., Park, M., Emmons, L., Kinnison, D., Bernath, P., Walker, K. A., Boone, C., and Pumphrey, H.: Asian monsoon transport of pollution to the stratosphere, Science, 328, 611–613, doi:10.1126/science.1182274, 2010. 18464, 18479

ACPD
14, 18461–18497, 2014

Riemer, M. and Jones, S. C.: Interaction of a tropical cyclone with a high-amplitude, midlatitude wave pattern: waviness analysis, trough deformation and track bifurcation, Q. J. Roy. Meteor. Soc., 140, 1362–1376, doi:10.1002/qj.2221, 2013. 18476

Riese, M., Grooß, J.-U., Feck, T., and Rohs, S.: Long-term changes of hydrogen-containing species in the stratosphere, J. Atmos. Sol-Terr. Phys., 68, 1973–1979, 2006. 18463

Riese, M., Ploeger, F., Rap, A., Vogel, B., Konopka, P., Dameris, M., and Forster, P.: Impact of uncertainties in atmospheric mixing on simulated UTLS composition and related radiative effects, J. Geophys. Res., 117, D16305, doi:10.1029/2012JD017751, 2012. 18463

Riese, M., Oelhaf, H., Preusse, P., Blank, J., Ern, M., Friedl-Vallon, F., Fischer, H., Guggenmoser, T., Höpfner, M., Hoor, P., Kaufmann, M., Orphal, J., Plöger, F., Spang, R., Suminska-Ebersoldt, O., Ungermann, J., Vogel, B., and Woiwode, W.: Gimballed Limb Observer for Radiance Imaging of the Atmosphere (GLORIA) scientific objectives, Atmos. Meas. Tech., 7, 1915–1928, doi:10.5194/amt-7-1915-2014, 2014. 18466

Röckmann, T., Grooß, J.-U., and Müller, R.: The impact of anthropogenic chlorine emissions, stratospheric ozone change and chemical feedbacks on stratospheric water, Atmos. Chem. Phys., 4, 693–699, doi:10.5194/acp-4-693-2004, 2004. 18463

Rohs, S., Schiller, C., Riese, M., Engel, A., Schmidt, U., Wetter, T., Levin, I., Nakazawa, T., and Aoki, S.: Long-term changes of methane and hydrogen in the stratosphere in the period 1978–2003 and their impact on the abundance of stratospheric water vapor, J. Geophys. Res., 111, D14315, doi:10.1029/2005JD006877, 2006. 18463

Rosenlof, K. H., Tuck, A. F., Kelly, K. K., Russell III, J. M., and McCormick, M. P.: Hemispheric asymmetries in the water vapor and inferences about transport in the lower stratosphere, J. Geophys. Res., 102, 13213–13234, 1997. 18463, 18464, 18478

Schiller, C., Krämer, M., Afchine, A., Spelten, N., and Sitnikov, N.: The ice water content of Arctic, mid latitude and tropical cirrus, J. Geophys. Res., 113, D24208, doi:10.1029/2008JD010342, 2008. 18467

Shindell, D. T.: Climate and ozone response to increased stratospheric water vapor, Geophys. Res. Lett., 28, 1551–1554, doi:10.1029/1999GL011197, 2001. 18463

Smith, C. A., Haigh, J. D., and Toumi, R.: Radiative forcing due to trends in stratospheric water vapour, Geophys. Res. Lett., 28, 179–182, 2001. 18463

Solomon, S., Rosenlof, K., Portmann, R., Daniel, J., Davis, S., Sanford, T., and Plattner, G.-K.: Contributions of stratospheric water vapor to decadal changes in the rate of global warming, Science, 327, 1219–1223, doi:10.1126/science.1182488, 2010. 18463

ACPD
14, 18461–18497, 2014

Vogel, B., Feck, T., and Grooß, J.-U.: Impact of stratospheric water vapor enhancements caused by CH_4 and H_2 increase on polar ozone loss, J. Geophys. Res., 116, D05301, doi:10.1029/2010JD014234, 2011a. 18463

Vogel, B., Pan, L. L., Konopka, P., Günther, G., Müller, R., Hall, W., Campos, T., Pollack, I., Weinheimer, A., Wei, J., Atlas, E. L., and Bowman, K. P.: Transport pathways and signatures of mixing in the extratropical tropopause region derived from Lagrangian model simulations, J. Geophys. Res., 116, D05306, doi:10.1029/2010JD014876, 2011b. 18475

Vogel, B., Feck, T., Grooß, J.-U., and Riese, M.: Impact of a possible future global hydrogen economy on Arctic stratospheric ozone loss, Energy Environ. Sci., 5, 6445–6452, doi:10.1039/c2ee03181g, 2012. 18463

Xiong, X., Houweling, S., Wei, J., Maddy, E., Sun, F., and Barnet, C.: Methane plume over south Asia during the monsoon season: satellite observation and model simulation, Atmos. Chem. Phys., 9, 783–794, doi:10.5194/acp-9-783-2009, 2009. 18463

Zahn, A., Weppner, J., Widmann, H., Schlote-Holubek, K., Burger, B., Kühner, T., and Franke, H.: A fast and precise chemiluminescence ozone detector for eddy flux and airborne application, Atmos. Meas. Tech., 5, 363–375, doi:10.5194/amt-5-363-2012, 2012. 18467

Zöger, M., Schiller, C., and Eicke, N.: Fast in situ hygrometers: a new family of balloonborne and airborne Lyman-α photofragment fluorescence hygrometers, J. Geophys. Res., 104, 1807–1816, 1999. 18467

ACPD
14, 18461–18497, 2014

Table 1. Number (N_{trajs}) and percentage of all trajectories in the region of interest, mean and maximum vertical velocity (calculated between 17 and 27 August 2012) along 40 day backward trajectories depending on levels of potential temperature at the air mass origin (Θ_{org}). The 40 day backward trajectories starting at the observation on 26 September 2012 and ending at the origin of the air masses in the past (17 August 2012). The air mass origins in terms of altitude and geographical position are also listed.

Θ_{org}	N_{trajs}	precentage	mean vertical velocity	max. vertical velocity	altitude origin	geographical position origin
295–320 K	8	2 %	very rapid uplift: 31 K day^{-1} (= 371 hPa day^{-1}) (= 6.6 km day^{-1}) 13 K/6 h (= 144 hPa/6 h) (= 2.5 km/6 h)	41 K day^{-1} (= 523 hPa day^{-1}) (= 9.4 km day^{-1}) 21 K/6 h (= 276 hPa/6 h) (= 3.7 km/6 h)	boundary layer	Southeast Asia
320–360 K	15	3 %	rapid uplift: 8 K day^{-1} (= 63 hPa day^{-1}) (= 2.3 km day^{-1}) 3 K/6 h (= 31 hPa/6 h) (= 1.1 km/6 h)	13 K day^{-1} (= 139 hPa day^{-1}) (= 4.4 km day^{-1}) 5 K/6 h (= 66 hPa/6 h) (= 1.9 km/6 h)	troposphere	mainly West Pacific
360–370 K	50	12 %	moderately rapid uplift: 2 K day^{-1} (= 22 hPa day^{-1}) (= 1.0 km day^{-1}) 1 K/6 h (= 11 hPa/6 h) (= 0.5 km/6 h)	5 K day^{-1} (= 41 hPa day^{-1}) (= 1.8 km day^{-1}) 2 K/6 h (= 25 hPa/6 h) (= 1.1 km/6 h)	AM anticyclone	mainly South Asia/North Africa
370–380 K	97	22 %	moderate uplift: 1 K day^{-1} (= 16 hPa day^{-1}) (= 0.8 km day^{-1}) 0.5 K/6 h (= 8 hPa/6 h) (= 0.4 km/6 h)	3 K day^{-1} (= 45 hPa day^{-1}) (= 2.3 km day^{-1}) 1 K/6 h (= 20 hPa/6 h) (= 1.0 km/6 h)	UTLS	mainly edge of the AM anticyclone
380–420 K	262	61 %	mainly descent		lower stratosphere	Northern Hemisphere

ACPD
14, 18461–18497, 2014

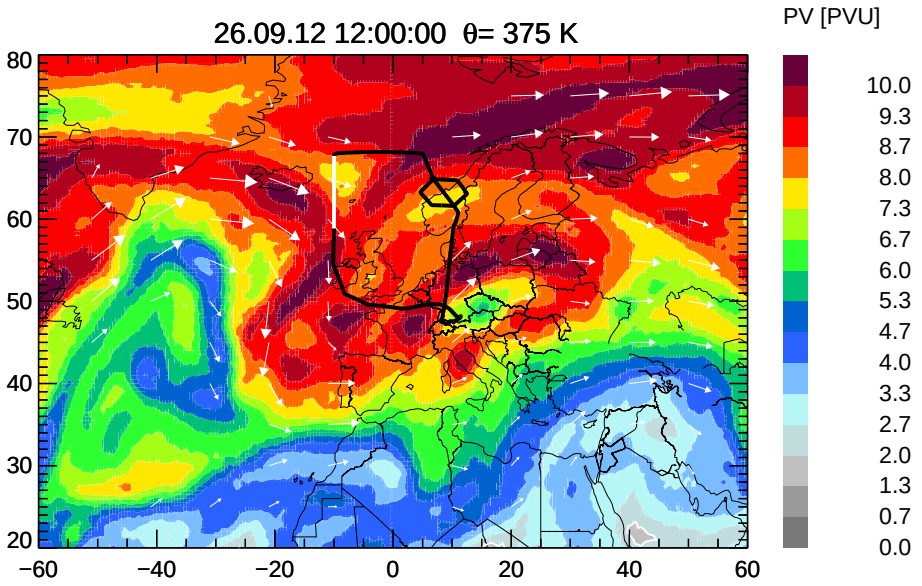

Figure 1. The horizontal distribution of PV at 375 K potential temperature over Northern Europe on 26 September 2012. The flight path for the TACTS flight on 26 September 2012 (at flight time) starting and ending in Oberpfaffenhofen (near Munich, 48° N 11° E, Germany) is marked in black. The part of the flightpath discussed within this paper is highlighted in white (cf. Sect. 2 and see Fig. 2). The horizontal winds are indicated by white arrows.

ACPD
14, 18461–18497, 2014

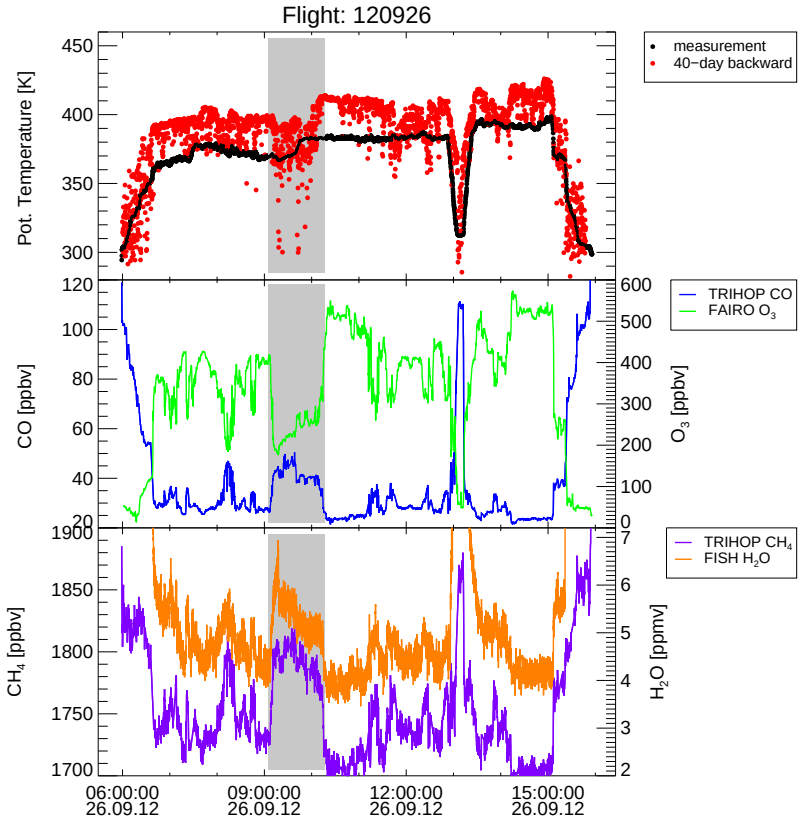

Figure 2. Time evolution (given in UTC time) of potential temperature, CO, O_3, CH_4, and H_2O measurements for the flight on 26 September 2012. Potential temperature values at the end points of 40 day backward trajectories (17 August 2012) are shown as red dots (upper panel). The part of the flightpath discussed within this paper is highlighted in grey (region of interest) (cf. Sect. 2 and see Fig. 1). Trajectories with origins (Θ_{org}) lower than 360 K potential temperature in the region of interest are shown in Fig. 3.

ACPD
14, 18461–18497, 2014

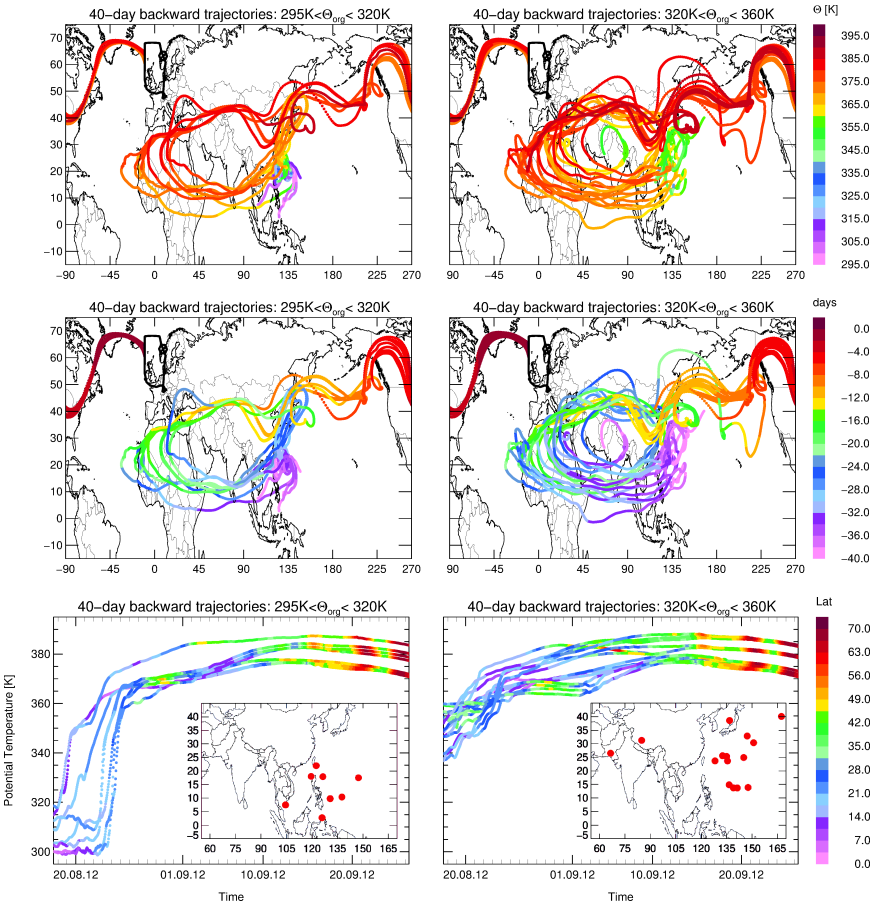

Figure 3.

ACPD
14, 18461–18497, 2014

Fast transport from Asian monsoon anticyclone to Europe

B. Vogel et al.

Figure 3. Different 40 day backward trajectories for Θ_{org} intervals 295–320 K (left) and 320–360 K (right) are shown colour-coded by potential temperature (top) and by days reversed from 26 September 2012 (middle). Further, potential temperature vs. time (in UTC) along 40 day backward trajectories (bottom) are shown. Here, the colour indicate the latitude position of the trajectories. The trajectory positions are plotted every hour (coloured dots). Large distances between single dots indicated very rapid uplift. The geographical position of the origins (Θ_{org}) of the 40 day backward trajectories (red dots) are shown in the embedded longitude-latitude-cut.

ACPD
14, 18461–18497, 2014

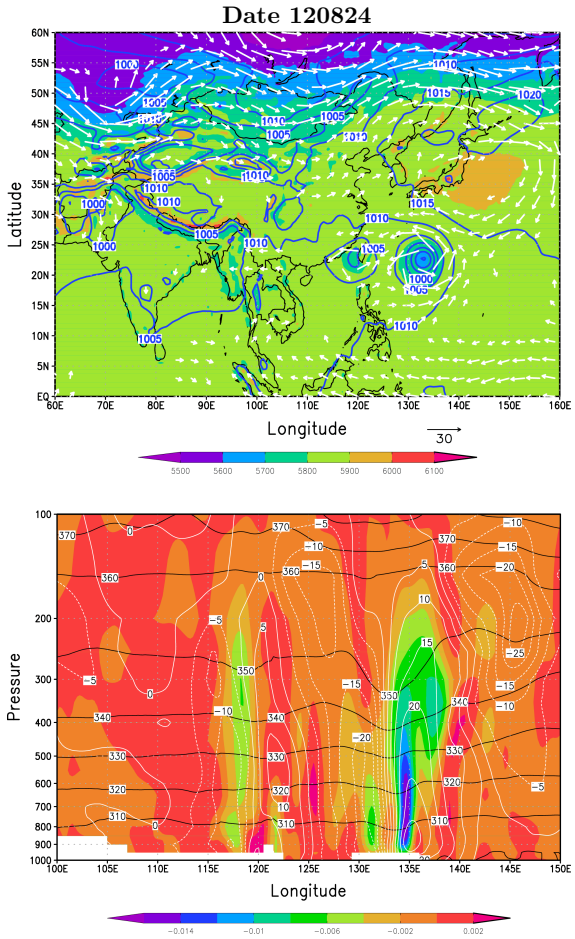

Figure 4.

ACPD
14, 18461–18497, 2014

Fast transport from Asian monsoon anticyclone to Europe

B. Vogel et al.

Figure 4. Geopotential height in [m] (colour) and horizontal winds in [ms^{-1}] (white arrows) at 500 hPa on 24 August 2012 (top). To show the position of the typhoons Tembin (≈ 23° N 118° E) and Bolaven (≈ 23° N 135° E) the mean sea level pressure in [hPa] is shown as blue thick lines. Longitude-height cross-section showing the typhoon Tembin and Bolaven at 23° N (bottom). The vertical velocity (ω) in [$hPa\,s^{-1}$] (colour), the horizontal winds in [ms^{-1}] (white line (positive values) and white dashed line (negative values)), and potential temperature in Kelvin (black lines) are shown. Very rapid uplift up to $-0.014\,hPa\,s^{-1}$ is found at the eastern flank of typhoon Bolaven (≈ 135° E) and up to $-0.006\,hPa\,s^{-1}$ is found at western flank of typhoon Tembin (≈ 118° E).

ACPD
14, 18461–18497, 2014

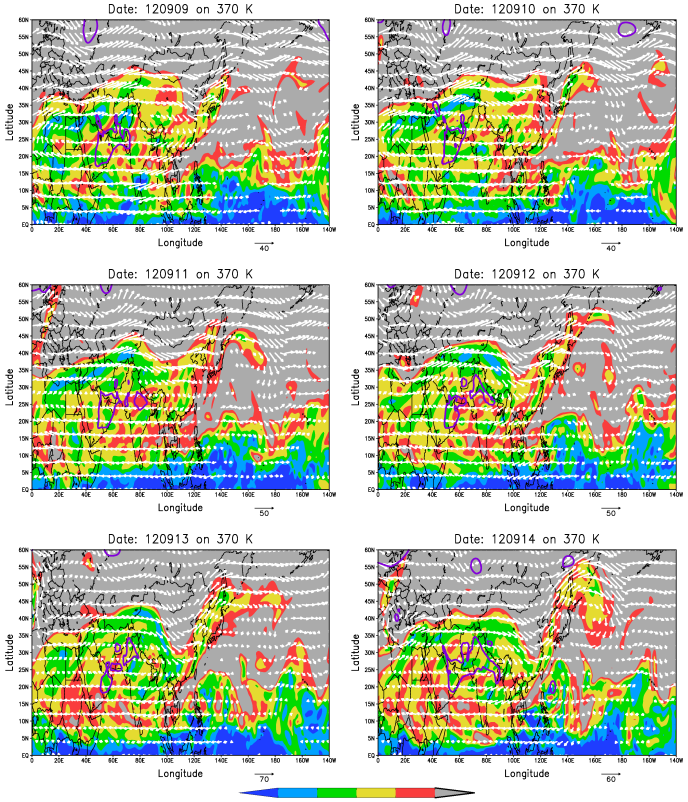

Figure 5. Time sequence of PV fields (colour shading in PVU) over Asia at 370 K potential temperature from 9 to 20 September 2012. The horizontal winds are indicated by white arrows. To show the position of tropospheric low-pressure systems in particular the super typhoon Sanba (e.g. ≈ 20° N 130° E on 14 September, ≈ 25° N 130° E on 15 September, ≈ 30° N 130° E on 16 September, and ≈ 40° N 130° E on 17 September) the sea level pressure of 1000 hPa is marked as thick purple line.

ACPD
14, 18461–18497, 2014

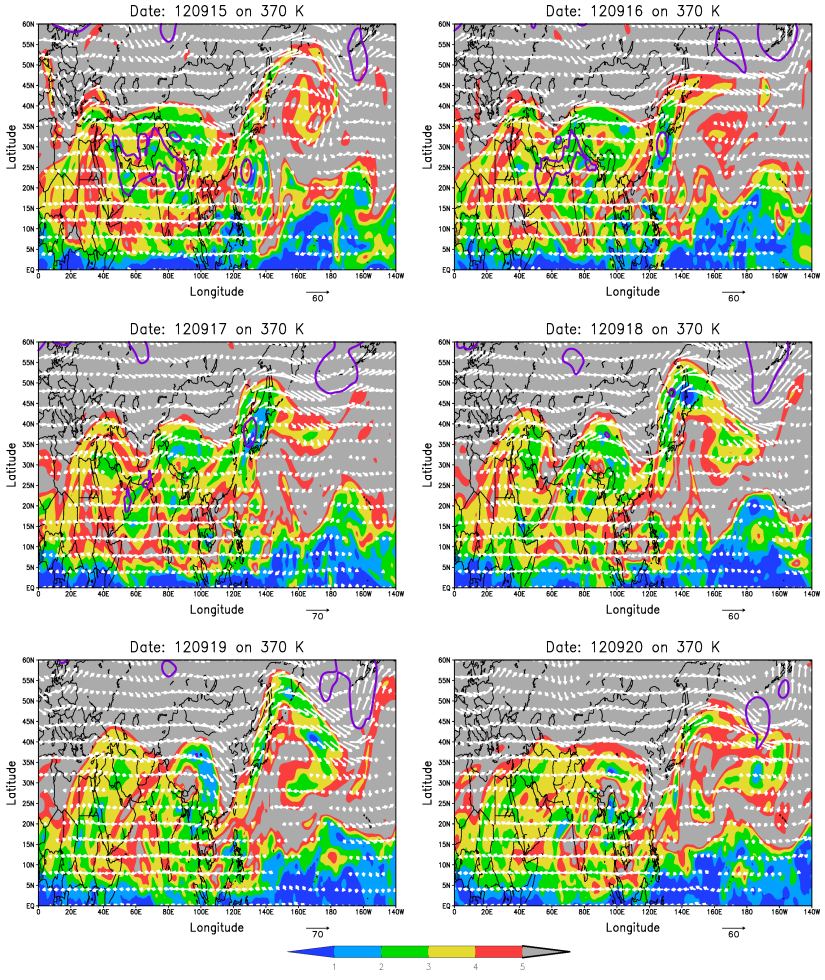

Figure 5. Continued.

ACPD
14, 18461–18497, 2014

Fast transport from Asian monsoon anticyclone to Europe

B. Vogel et al.

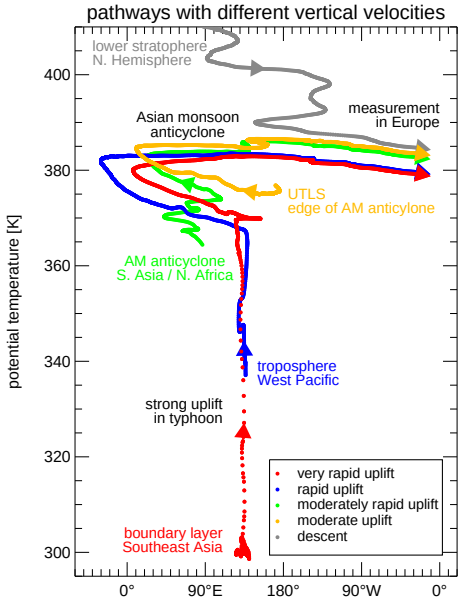

Figure 6. Selected trajectories representing characteristic pathways with different vertical velocities (cf. Table 1) as function of potential temperature and longitude for the time period between 17 August and 26 September 2012. The air mass positions are plotted every hour (coloured dots). Large distances between the single dots indicated very rapid uplift. The classification of the different vertical velocities is derived for the first ten days of the trajectories (17–28 August 2012). For simplification longitudes between 60° W and 20° E are shown twice. The coloured text gives information about the altitude origin and geographical position origin of the different pathways. The figure illustrates different transport pathways of air masses with different origin to the location of the measurement over Northern Europe. The combination of very rapid uplift by a typhoon and eastward eddy shedding from the Asian monsoon anticyclone yield fast transport (≈ 5 weeks) from Southeast Asia boundary layer sources to Northern Europe (red).

ACPD
14, 18461–18497, 2014